R. KIENBERGER[1],✉

M. HENTSCHEL[1]

C. SPIELMANN[1]

G.A. REIDER[1]

N. MILOSEVIC[1]

U. HEINZMANN[2]

M. DRESCHER[2]

F. KRAUSZ[1]

# Sub-femtosecond X-ray pulse generation and measurement

[1] Institut für Photonik, Technische Universität Wien, Gusshausstr. 27, 1040 Wien, Austria
[2] Fakultät für Physik, Universität Bielefeld, 33 615 Bielefeld, Germany

**ABSTRACT** We report the generation and measurement of isolated soft-X-ray pulses ($\lambda_X = 14$ nm) with a duration of $\tau_X = 650 \pm 150$ attoseconds (as) by using few-cycle intense visible/near-infrared ($\lambda_0 = 750$ nm) laser pulses. For the temporal characterization of the X-ray pulses, a cross-correlation technique relying on laser field assisted X-ray photoemission from krypton atoms was employed. The experimental results bear direct evidence of the X-ray pulse being synchronized to the field oscillations of the visible-light pulse with attosecond precision and of bound–free electronic transitions from the $4p$ state of krypton responding to 90-eV excitation on an attosecond time scale. As a first demonstration of attosecond metrology, the synchronized single sub-fs X-ray pulses were used for tracing the electric field oscillations in a visible-light wave with a resolution of better than 150 as.

**PACS** 32.80.Fb; 42.55.Vc; 42.65.Ky; 42.65.Re

## 1 Introduction

The interest in ultra-fast microscopic processes is the driving force behind the development of sources and measurement techniques that allow time-resolved studies at ever shorter time scales. In the classical scheme of time-resolved experiments, a short excitation pulse setting the process going and a short probe pulse for taking snapshots of subsequent stages of its evolution constitute the basis for gaining experimental access to fast-evolving microscopic processes. Recent advances in ultra-fast optics made laser pulses as short as a few femtoseconds [1–6] available for these pump–probe measurement techniques.

Currently available laser pulse durations are practically at the limit set by the laser field oscillation cycle, which lasts somewhat longer than one femtosecond (1 fs = $10^{-15}$ s) in the visible spectral range. Coherent extreme ultraviolet (XUV) and X-ray sources [7–10] offer, owing to their short wave cycle, the potential for producing electromagnetic radiation of attosecond (as) duration [11–14]. Using few-cycle visible laser pulses [15] for both the generation of isolated soft-X-ray

✉ E-mail: reinhard.kienberger@tuwien.ac.at

harmonic pulses and their temporal characterization in a novel cross-correlation technique [16], we have demonstrated the existence of sub-femtosecond electromagnetic pulses for the first time [17]. In this paper we review these recent developments, concentrating on the measurement of ultra-short XUV/X-ray pulses. For an extended review of the generation of such pulses, see e.g. [18].

## 2 XUV/X-ray pulses by high-order harmonic generation

In our experiments coherent high-harmonic generation (HHG) is accomplished by focusing 0.7-mJ linearly polarized ≈ 750-nm laser pulses of 7-fs duration at a 1-kHz repetition rate [19] into a volume of Ne gas (see photograph in Fig. 2) [20]. The pulses originate from a dispersion-controlled, Kerr-lens-mode-locked Ti:sapphire oscillator delivering sub-10-fs pulses at a repetition rate of approximately 80 MHz. After being temporally stretched by a 10-cm slab of SF57 glass these pulses are passed through a multi-pass Ti:sapphire amplifier in a confocal geometry. When pumped with ∼ 10-mJ pulses at a 1-kHz repetition rate by a Q-switched, frequency-doubled, lamp-pumped Nd:YLF laser, the amplifier boosts the pulse energy to typically 1.5–1.7 mJ in 10 passes through the amplifier crystal. Amplification is followed by recompression to a duration of typically 20–25 fs by two pairs of fused-silica Brewster prisms. The compressor throughput is higher than 90% and results in a pulse energy of 1.3–1.5 mJ [21].

For further compression the pulses are focused into a hollow-core fused-silica fiber with an inner diameter of 250 µm and a length of 1 m. The fiber is filled with neon at ∼ 1 bar, which imposes a dynamic phase shift on the pulse propagating down the waveguide due to the optical Kerr effect. The frequency broadening induced in this manner is converted into temporal compression by a set of broadband chirped dispersive mirrors, yielding pulse durations down to 5–7 fs. The finally available pulse energy is typically 0.5–0.7 mJ, corresponding to a peak power of around 0.1 TW.

For the process of HHG, the laser beam is focused into a vacuum chamber by a silver-coated spherical mirror through a 0.3-mm-thick fused-silica window. Near the focus of the beam, neon atoms effusing from holes drilled into a Ne-backed Ni tube by the focused laser beam are exposed to

peak electric fields of $\approx 8.8 \times 10^{14}$ W/cm$^2$ over an effective interaction length of $\approx 3$ mm. They emit coherent soft-X-ray harmonic radiation up to photon energies exceeding 100 eV [20]. Maximum yield at 90-eV photon energy is achieved at a backing pressure of 0.2 bar. The chamber is pumped by a roots pump to keep the background pressure in the range of $10^{-2}$ mbar.

The soft-X-ray photons are delivered in a well-collimated beam (divergence $\approx 1$ mrad) from the X-ray-source chamber through a miniature beamline into the target chamber. The beamline connecting the generation chamber with the target chamber is pumped by a 330 $\ell$/s turbo-molecular pump and separated by an aperture and a Zr filter from the two chambers, respectively. The target chamber is evacuated by a 800 $\ell$/s turbo-molecular pump to a pressure of about $10^{-6}$ mbar.

## 3 Cross correlation of the X-ray pulse with a few-cycle laser field

The temporal characterization of the generated broadband (multi-eV-bandwidth) XUV/soft-X-ray pulses produced by HHG sources turns out to be a formidable challenge, since conventional auto-correlation schemes based upon second-order nonlinearities require photon fluences orders of magnitude higher than those available from existing HHG sources. We have recently proposed and demonstrated a novel cross-correlation technique based on X-ray photoionization in the presence of an intense few-cycle laser field [16, 17]. It is based on the effect that the final kinetic energy of X-ray-generated photoelectrons is controlled by the oscillating light field at the instant of ionization. The features (width and position) of the resulting photoelectron spectra as a function of the relative delay between X-ray and laser pulses are determined by a convolution of the laser light field and the X-ray pulse envelope. Careful deconvolution allows us to evaluate the duration of the X-ray pulse and its timing jitter with respect to the light field on an attosecond time scale.

Experimentally, photoelectrons from atoms exposed simultaneously to a strong light field and an X-ray pulse are detected with a time-of-flight (TOF) spectrometer. The detection cone is aligned orthogonally to the electric field vector of the linearly polarized laser field, in order to suppress a background in the photoelectron spectrum originating from above-threshold ionization (ATI) of the atoms by the laser. In the strong-field limit, a quasi-classical model summarized in Sect. 3.1 takes proper account of the modifications of the photoelectron spectrum by the laser field.

In the framework of this model, the photoelectron is first ejected by a short X-ray pulse with a distribution of initial momenta known from conventional photoionization studies [22]. Subsequently, it is accelerated (or decelerated) by the light field. For X-ray pulse durations $\tau_X$ very short compared to $T_0/2$, the model predicts that, depending on the oscillation phase of the light field at the instant of 'birth' of the electron, a momentum component along the electric field vector is added to the initial momentum of the electron, resulting in a shift of the photoelectron angular distribution up or down in momentum space (Fig. 1). The width of the X-ray photoelectron energy spectrum $\Delta W$, which is equal to the bandwidth of the X-ray pulse spectrum in the absence of the light field, increases with increasing momentum shift.
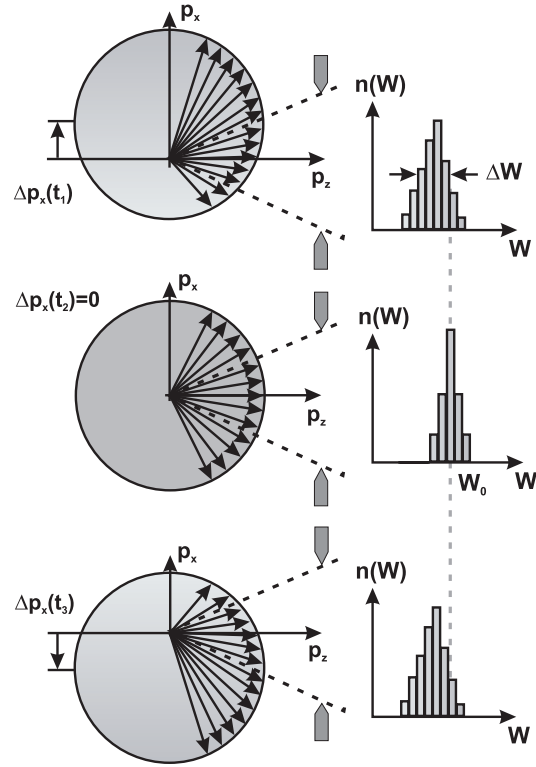


FIGURE 1 Principle of measuring light-field/X-ray-intensity cross correlation with attosecond resolution. The photoelectrons created initially with isotropic momentum distribution by the absorption of X-ray photons pick up a momentum from the strong laser light field. The light-induced momentum change $\Delta p_x$ deforms the final photoelectron momentum distribution at instants $t_1$, $t_2 = t_1 + T_0/4$ and $t_3 = t_1 + T_0/2$ as shown, where $E_L(t_1) = E_L(t_3) = 0$. Photoelectrons detected within a cone aligned orthogonally to the direction of the light field vector ($x$ direction) display a kinetic energy spread at $t_1$ and $t_3$ whilst remaining unaffected by the light field at $t_2$

As the analysis in Sect. 3.1 shows, scanning the instant of birth of the photoelectron through the light field oscillations by changing the relative delay $t_d$ between the light pulse and the X-ray pulse results in a modulation of the center of gravity as well as the width $\Delta W(t_d)$ of the X-ray photoelectron spectrum with a period equal to one-half of the light oscillation period $T_0$. For sub-femtosecond X-ray pulse measurement we shall exploit the field-induced spectral broadening [17] because this effect is enhanced by increasing the detection aperture as revealed by Fig. 1, resulting in a significantly enhanced signal yield and modulation amplitude of $\Delta W(t_d)$. By contrast, a modulation in the kinetic energy shift gets increasingly washed out with increasing detection angle, deteriorating the temporal resolution.

### 3.1 Light-field-controlled X-ray photoemission

Our method of measuring a cross correlation between an X-ray pulse and a visible laser pulse can be summarized as laser-light-assisted X-ray photoionization. The basic idea is to overlap the two pulses with variable delay with respect to each other in a gas medium and to measure the kinetic energy of the photoelectrons stripped off the atoms by the X-ray pulse. Taking advantage of the semi-classical approach outlined above, the motion of an X-ray-induced photoelectron 'born' at a delay time $t_d$ with respect to the peak of the laser

pulse is governed by the classical equation of motion. Along the direction of laser polarization ($x$) this equation reads

$$m\dot{v}_\parallel = qE_L = -eE_a(t)\cos\omega_L t. \tag{1}$$

In the adiabatic limit ($dE_a(t)/dt \ll E_a(t)\omega_L$) the femtosecond laser pulse changes the velocity of the electron by

$$\Delta v_\parallel = \frac{e}{m}\frac{E_a(t_d)\sin\omega_L t_d}{\omega_L} = \sqrt{\frac{4U_p(t_d)}{m}}\sin\omega_L t_d, \tag{2}$$

$$\Delta v_\perp = 0 \tag{3}$$

in the directions parallel and perpendicular to the laser polarization, respectively. Here

$$U_p = \frac{e^2 E_a^2(t_d)}{4m\omega_L^2} \tag{4}$$

is the time-averaged electron wiggling energy. This change of the initial velocity of the electron results in a modification of the final kinetic energy $W_f$. For $U_P \ll W_0$ the final energy is given by

$$W_f \approx W_0 + 2U_p(t_d)\sin^2\omega_L t_d \cos 2\theta$$
$$+ \sqrt{8W_0 U_p(t_d)}\sin\omega_L t_d \cos\theta, \tag{5}$$

where $W_0 = \hbar\omega_X - W_b$ is the initial kinetic energy of the photoelectron, $\omega_X$ denotes the X-ray photon energy, $W_b$ stands for the atomic binding energy of the electron liberated ($\hbar\omega_X \gg W_b$) and $\theta$ is the angle between the final momentum of the electron and the laser electric field vector.

In order for the predicted variation of the photoelectron kinetic energy as a function of $t_d$ to be compared with measurements, (5) needs to be generalized for a finite emission time slot of the photoelectron (corresponding to the finite X-ray pulse duration) and for a distribution of initial kinetic energies over a finite energy range (reflecting the finite bandwidth of the X-ray pulse). In addition, the distribution of final kinetic energies as a function of $\theta$ has to be integrated over the finite detection cone to obtain a realistic prediction for the measured X-ray photoelectron spectrum modified by the laser field.

For an X-ray pulse short compared to half the laser period, i.e. $\tau_X \ll T_0/2$, and a fast (attosecond) response of the electronic transitions involved in the process, the predicted modulations in the final kinetic energy distribution versus $t_d$ survive these integrations and provide a sub-femtosecond probe for the measurement of the X-ray pulse duration. A finite X-ray pulse duration or a finite timing jitter of the X-ray pulse (relative to the phase of the light field) of any origin results in a reduced depth of the resultant modulation of the width and center of gravity of the photoelectron energy spectrum (illustrated in Fig. 1). In fact, an X-ray pulse duration or a timing jitter exceeding $T_0/2$ ($\sim 1.25$ fs in our case) smears out the modulation completely. The claim of a sub-femtosecond pulse duration relies on this line of argument: the modulation depth of $\Delta W(t_d)$ provides a reliable upper limit, on an attosecond time scale, for X-ray pulse duration and timing jitter.

### 3.2    Setup

Figure 2 displays the setup of our experiment. The X-ray pulses exiting the neon harmonic source co-propagate with the laser pulses down the beam-delivery tube. After 150 cm they hit a 200-nm-thick zirconium foil with an aperture of 2 mm mounted on a nitrocellulose membrane of 5-μm thickness. This filter, which is virtually dispersion-free at the laser wavelength, produces an annular laser beam with the X-ray beam in the center. The energy in the laser beam is adjusted by a motorized iris and measured by a photodiode. Both the laser and the X-ray pulses are focused with a special multi-purpose mirror with a focal length of 35 mm. This mirror is mounted on a motorized stage so that it can be removed from the beamline. In this way the harmonic beam can be detected by a multi-channel plate (MCP) for optimizing the radial intensity profile of the X-ray beam (by fine adjustment of the position and pressure of the neon-gas target and of the intensity of the laser pulses).

The mirror is coated with a Mo/Si multi-layer stack designed to reflect photons with 90-eV energy within a 5-eV bandwidth. This bandwidth is large enough to support X-ray pulses as short as 0.4 fs. The mirror substrate consists of two concentric parts, matching the impinging laser and X-ray beam. The central piece is sitting on a piezo stage adjustable in transverse and longitudinal directions. In this manner the two pulses can be overlapped spatially and temporally in the focal plane, where a nozzle supplying the target atoms is situated.
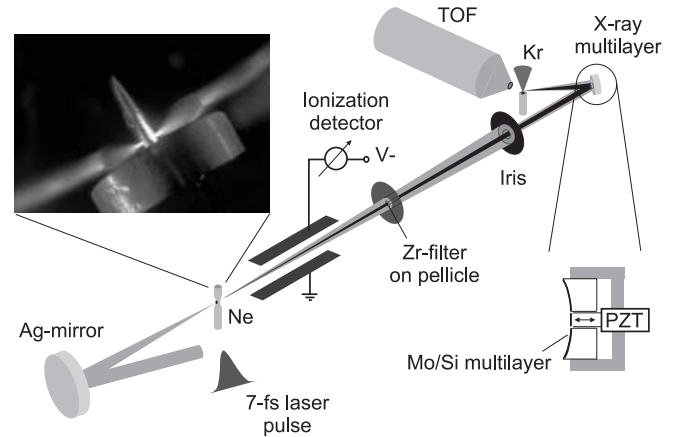


**FIGURE 2**   The schematic of the experiment. The focused 7-fs laser beam interacts with neon atoms to produce high-harmonic radiation. The laser and the highly collimated X-ray beam co-propagate collinearly through a 2-m beamline towards the measurement region. Differential pumping stages reduce the pressure from $\approx 4\times 10^{-2}$ mbar in the source chamber to the range of $\approx \times 10^{-5}$ mbar in the target chamber. An ionization detector in the higher-pressure part of the beamline serves for monitoring the (spectrally integrated) high-harmonic flux. In the beamline the laser and harmonic beams pass through a 200-nm thick, 3-mm-diameter zirconium foil placed on a 5-μm-thick nitrocellulose pellicle to cover a hole of 2-mm diameter. The energy transported by the resulting annular beam can be adjusted with a motorized iris between a fraction of a microjoule and a few tens of microjoules. The Mo/Si multi-layer consists of an annular part having an outer diameter of 10 mm with a concentric hole of 3-mm diameter hosting a miniature mirror of slightly smaller diameter. Both parts originate from the same substrate, ensuring identical radii of curvature ($R = 70$ mm). The miniature central mirror is mounted on a quadrant piezo stage, allowing alignment and translation with respect to the external part

The profile of the laser focus can be imaged by a lens on a CCD camera for monitoring and coarse preadjustment of spatial overlap between the beams reflected by the two components of the Mo/Si mirror. Krypton atoms effusing from the orifice of the nozzle (diameter 50 μm) with a rate of 0.02 mbar ℓ/s are photoionized by the X-ray pulses in the presence of the laser field. To avoid a constant photoelectron background due to ionization by the unfocused X-ray beam, a thin shield is placed next to the krypton target. All parts in the vicinity of the spectrometer are conductively coated and properly grounded to avoid electrostatic charging.

The entrance aperture of the time-of-flight photoelectron spectrometer (Fig. 3) having a diameter of 5 mm is placed at a distance of approximately 5 mm from the interaction region. The TOF spectrometer can be mechanically adjusted to optimize the acceptance angle and to center the electron source on the tube axis. The relatively large numerical aperture (NA ∼ 1) of our TOF spectrometer is due to a carefully designed grid-free collecting electrostatic lens system optimized for the energy region of 50–100 eV, which has resulted in an order-of-magnitude improvement of detection efficiency as compared to conventional TOF tubes. Owing to the absence of meshes in the electron path, distortion of the trajectories due to microlensing by inhomogeneous electric fields close to the grid is avoided.

The electrostatic lens system consists of six concentric rings set to different electric potentials ($U_{1-6}$) bending the electron trajectories towards the axis. The adjacent flight tube is magnetically shielded to avoid deflection of the electrons due to stray magnetic fields. Application of a retarding voltage of −20 V to the 40-cm-long five-metal-shielded drift tube improves the energy resolution by lowering the electron velocity. The spectrometer can be operated to provide almost flat transmission for kinetic energies ranging from 40 eV to 80 eV. However, in order to optimize the sensitivity for the Kr-4$p$ photoline the lens voltages were chosen to obtain maximum transmission at ∼ 75 eV with a cut-off above 100 eV. Under these conditions the spectral resolution is still better than 1 eV.

Particular attention has been paid to a careful choice of the electronic acquisition system for the transient signal from the electron detector at the rear of the TOF drift tube. If directly acquired with a digital oscilloscope, the resulting waveform actually represents a convolution of the electron spectrum with the temporal response of the microsphere plate (MSP) detector to a single-electron event in the time domain. Even if the detector anode is carefully designed to avoid pulse distortion and ringing the achievable temporal resolution with

this technique will not exceed 1–2 ns. If needed, substantially improved resolution (down to some 200 ps) is possible with time-resolved single-event counting by evaluating the rising edge of the detector pulse in a constant-fraction discriminator followed by a time-to-amplitude converter (TAC), an analog-to-digital converter and a multi-channel analyzer.

During data acquisition each laser pulse generates the start trigger for a time-to-amplitude converter via a photodiode. The stop pulse is derived from the MSP detector signal. The output of the TAC is read out by a computer and accumulated in a multi-channel pulse-height analyzer. The resulting flight-time spectrum has a resolution of $\tau = 0.464$ ns/channel with 1024 channels in total. The time scale is converted to energy according to

$$E = \left[ \frac{L_{\text{eff}}}{((i + i_0)\tau - \tau_0)} \right]^2 + U_{\text{eff}}, \qquad (6)$$

with $i$ being the channel number and $i_0$ depending on the length of the start trigger line and the internal delay of the TAC. $L_{\text{eff}} = 501.01$ ns·eV$^{1/2}$ is the length of the flight tube weighted with the square root of the effective electron mass, $\tau_0 = 12.01$ ns a correction of the flight time and $U_{\text{eff}} = -19.36$ eV the effective potential caused by the retardation voltage $U_{\text{ret}} = -20$ V. Alternatively the flight-time spectra can be recorded with a fast oscilloscope (TDS 520 D, Tektronix).

### 3.3    *Measurement*

Before the X-ray/laser-field cross correlation can be recorded by measuring the X-ray photoelectron spectrum as a function of $t_d$ the temporal overlap between the two pulses has to be found. To this end, we generate ATI electrons upon removing the Zr filter (stopping the central fraction of the laser beam) from the beamline and by focusing both the inner and the annular parts of the laser beam with the two-component Mo/Si multi-layer mirror onto the krypton target. Scanning the delay between outer and inner parts of the mirror with a feedback-controlled piezo translator, an 'interferometric' ATI autocorrelation of the 7-fs laser pulse can be recorded. Figure 4 shows the detected electron count rate as a function of the delay between the two replicas of the laser pulse. Owing to the strongly nonlinear dependence of the ionization rate on the electric field strength and the few-femtosecond pulse duration, the trace is confined to virtually a single laser cycle. The central peak indicates the delay of optimum temporal overlap between the two beams. From this reference, the zero delay between the X-ray and laser pulses can be inferred by taking into account the finite (≈ 5 μm) thickness of the pellicle holding the Zr foil, which is reintroduced for the X-ray/laser-field cross-correlation measurements.

The delay $t_d$ was varied in steps of $\Delta t_d = 150$ as in the central range of temporal overlap ($-5$ fs $\leq t_d \leq 5$ fs, with $t_d = 0$ approximately at the peak of the light pulse) and of increased step size outside this range. The inset in Fig. 5 shows two representative Kr-4$p$ spectra corrected for (a constant) ATI background and recorded at $t_d = -450$ as and $t_d = 0$ as, along with respective asymmetric Gaussian fits. This model function yields excellent fits to our data, characterized by a fidelity
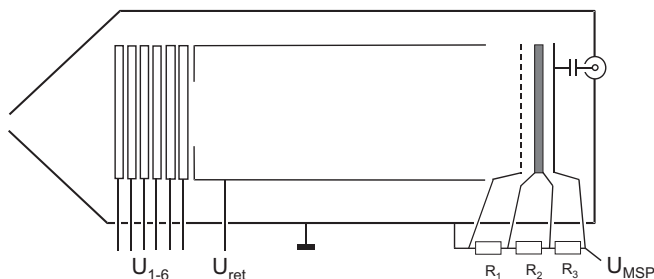


**FIGURE 3**    Schematic of the time-of-flight electron spectrometer. Overall length is 40 cm, tube diameter is 6 cm. $R_1 = R_3 = 3.3$ MΩ, $R_2 = 22$ Ω
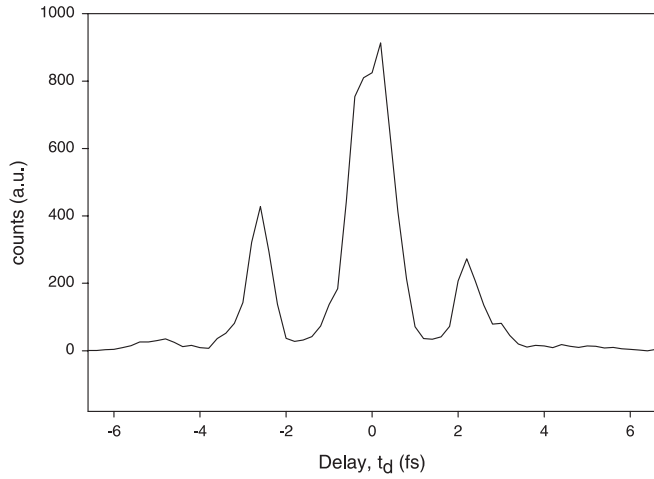
**FIGURE 4**   ATI electron autocorrelation

parameter $R^2 > 0.95$. The noise increasing to lower energies can be attributed to ATI electrons. The upper graph in Fig. 5 depicts a series of Kr-$4p$ photoelectron spectra (processed as described above) as a function of delay $t_d$. The plot comprises some 120 spectra of the $4p$ feature, each normalized to the same number of counts, resulting in a constant area under the spectral distribution functions. Owing to the relatively large solid angle of detection the overall measurement time could be limited to $\sim 5$ h. The data clearly bring to light a quasi-periodic evolution of the photoelectron energy spectrum at a period of $\sim T_0/2$. In this representation the most pronounced modulation versus $t_d$ appears at the peak of the spectra. With the total number of electrons per spectrum fixed, this is a direct consequence of the modulation of spectral width.

The dots in Fig. 5 depict the width $\Delta W(t_d)$ as evaluated from the Gaussian fits introduced above. From an inspection of the error bars at points of maximum slope in Fig. 5 we infer a time resolution of $\sim 150$ as. The modulation period of the

data is close to 1.25 fs in the wings of the correlation function $\Delta W(t_d)$, in agreement with a carrier wavelength of $\sim 750$ nm of the light pulse. However, it decreases to $\sim 1$ fs near zero delay, indicative of a pronounced blue shift of the light pulse at its peak, the origin of which we shall discuss below. With our large-aperture detection, a shift of the spectral 'center-of-gravity' is observed. In agreement with our model, the modulation of this shift is synchronous with that of $\Delta W(t_d)$ but turns out to be contaminated with much (factor of 2–3) larger errors.

## 4      Isolated sub-femtosecond X-ray pulses

For evaluating the X-ray pulse duration from our light-field/X-ray-intensity cross-correlation data (dots in Fig. 5) we introduce a measure for the depth of modulation of $\Delta W(t_d)$, the fringe visibility

$$\text{FV} = (\Delta W_{\max} - \Delta W_{\min})/(\Delta W_{\max} + \Delta W_{\min} - 2\Delta W_\infty), \quad (7)$$

where $\Delta W_{\max}$ and $\Delta W_{\min}$ stand for adjacent local extremal values of $\Delta W(t_d)$ as a function of the delay time and $\Delta W_\infty = \Delta W(t_d \to \infty)$, and measure the local fringe spacing (FS). The central portion of the correlation function $\Delta W(t_d)$, with maximum FV and minimum FS, provides optimum resolution for determining the X-ray pulse duration. A sinusoidal fit to the two central modulation periods (dots in Fig. 5) yields FS $= 960 \pm 30$ as and FV $= 0.30 \pm 0.03$.

For comparison with the measured data Fig. 5, we simulated the light-field-induced variation of the Kr-$4p$ photoelectron spectrum versus $t_d$ based on the quasi-classical model described above. The duration $\tau_X$ of our Gaussian model X-ray pulse was used as the only fit parameter. The visible-light pulse was also modeled with a Gaussian intensity envelope peaking at $10^{14}$ W/cm$^2$, carrying a quadratic frequency sweep to account for the frequency upshift present at the center of the measured correlation function $\Delta W(t_d)$. Best agreement with the data in Fig. 5 was achieved for X-ray pulse durations in
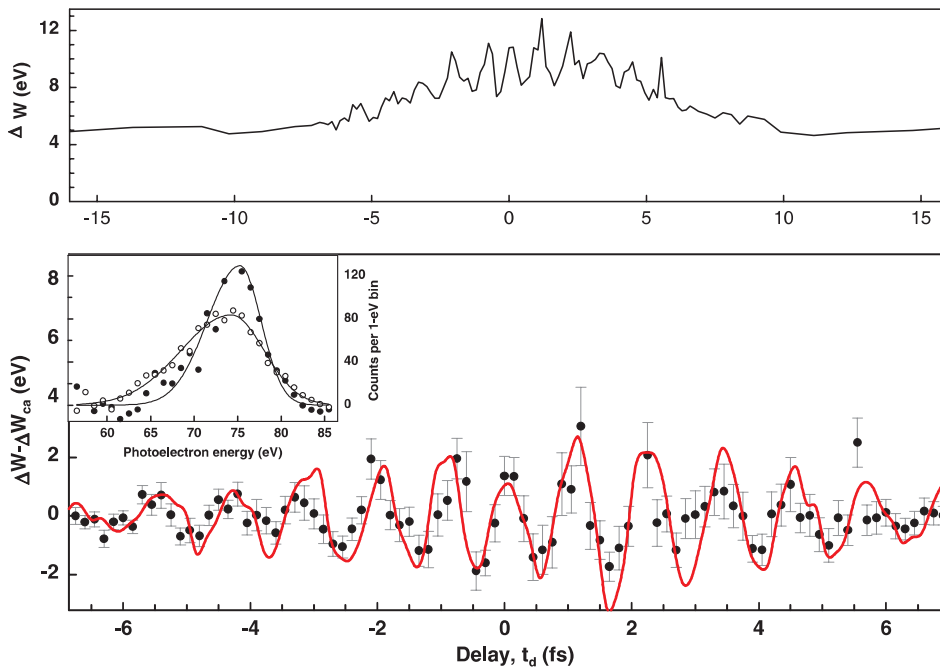


**FIGURE 5**   Spectral width $\Delta W$ of the Kr-$4p$ photoelectron spectra (evaluated from the asymmetric Gaussian fits) as a function of the delay $t_d$ between the light wave and the X-ray pulse. The *dots* represent the oscillating component of the spectral width, $\Delta W - \Delta W_{ca}(t_d)$, where $\Delta W_{ca}(t_d)$ stands for the cycle-averaged value of $\Delta W(t_d)$. The *full line* is the result from simulations based on the quasi-classical theory of two-color X-ray photoionization by assuming a frequency-swept (see text), 7-fs, 750-nm linearly polarized light field of $5 \times 10^{13}$ W/cm$^2$ peak intensity and a 650-as, 90-eV Gaussian X-ray pulse. *Upper graph*, spectral width $\Delta W$ evaluated from the Gaussian fits as a function of the delay $t_d$. *Inset*: Kr-$4p$ photoelectron spectra produced by $\sim 90$-eV X-ray pulses in the presence of a strong visible light field at two different delays of the X-ray pulse with respect to the light wave. The *dots* represent spectra corrected for some ATI background from the measurements performed by a time-of-flight electron spectrometer. The *lines* show asymmetric Gaussian fits to the data

the range of 600 as $\leq \tau_X \leq$ 700 as, yielding a fringe visibility of FV $= 0.30 \pm 0.05$ in the correlation function near $t_d = 0$ as. Assuming pulse durations of $\tau_X = 500$ as and $\tau_X = 800$ as, respectively, the FV is enhanced and suppressed with respect to the measured value well beyond the experimental error of
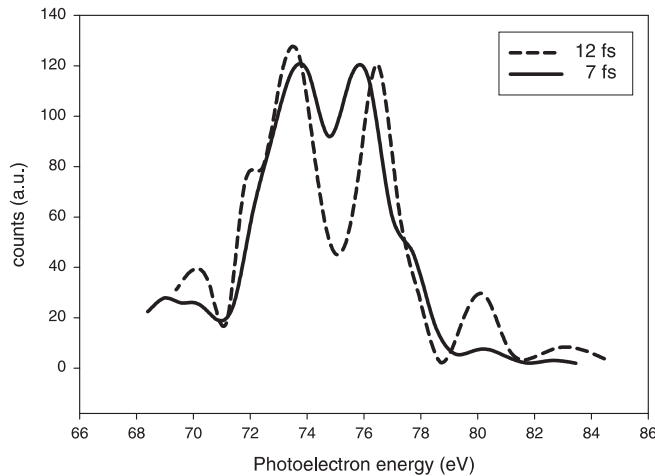


**FIGURE 6** Photoelectron spectra of X-ray pulses generated by 7-fs respectively 12-fs laser pulses
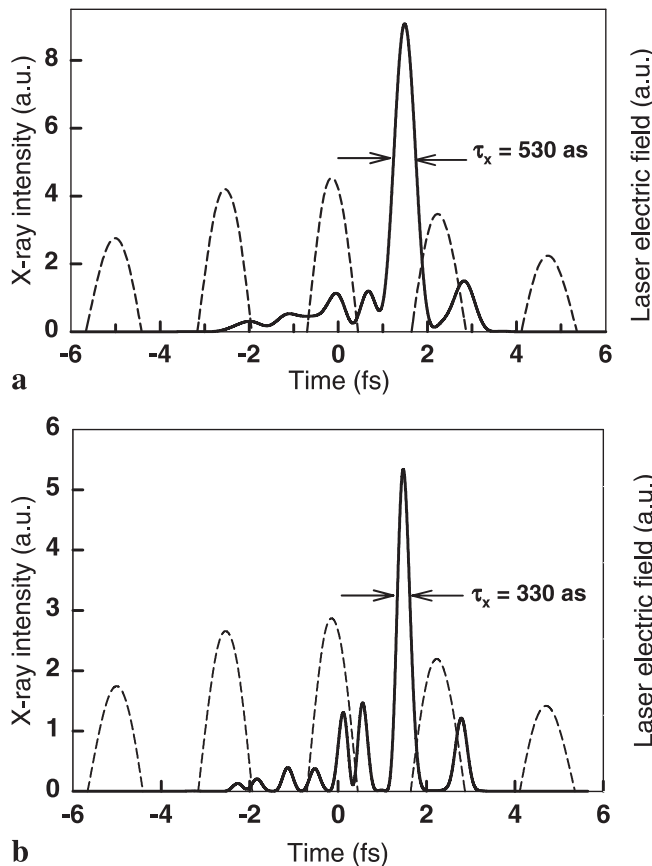


**FIGURE 7** Calculated far-field, near-axis temporal intensity profile of soft-X-ray harmonic radiation (*full line*) selected within the spectral range of **a** $90\pm 2.5$ eV and **b** $90\pm 5$ eV, produced in a 3-mm-long 200-mbar neon-gas volume by a 7-fs, 750-nm Gaussian laser pulse $E(t) \propto \exp(-t^2/\tau_L^2) \cos(\omega_0 t + \varphi)$ with $\varphi = 0$ (cosine pulse) and an on-axis peak intensity of $8 \times 10^{14}$ W/cm$^2$. The *dashed line* shows the on-axis electric field of the laser pulse exiting the interaction region

10%. Therefore, $\tau_X = 650 \pm 150$ as represents a safe estimate for the duration of our 90-eV X-ray pulse. The sensitivity of the method is underlined by the computed FV decreasing by a factor as large as three (from 0.30 to 0.10) as the X-ray pulse duration is increased from 650 as to 900 as, with the modulation in $\Delta W(t_d)$ disappearing for $\tau_X \geq 1$ fs.

An essential question is whether this sub-femtosecond pulse is accompanied by one or more satellite pulses spaced by $\sim T_0/2$ as observed in a recent experiment [12]. A concomitant of the emergence of equidistant satellite pulses is the appearance of spectral sidebands (at twice the photon energy of the driver laser) of rapidly increasing magnitude with increasing weight of the satellite pulse(s). The absence of any significant modulation in our X-ray harmonic spectrum reflected by the Mo/Si multi-layer limits the possible satellite fluence to less than 10% of the total X-ray fluence. Figure 6 shows the measured photoelectron spectra, full and dashed lines, reflecting those of the generating X-ray pulses produced laser pulses of 7 fs and, for comparison, 12 fs in duration, respectively. The latter spectrum indicates that the weak modulation of the 7-fs pulse-produced X-ray spectrum is not due to finite spectral resolution of the TOF detector. Further confirmation of the low weight of X-ray satellite pulses is supplied by results summarized in Sect. 5.

The emergence of a single sub-femtosecond pulse from high-harmonic generation in the few-cycle regime as realized in our experiment was corroborated by preliminary numerical studies based on a computer code [23] solving Maxwell's wave equations in three dimensions and calculating the radiation of the strongly driven atomic dipoles using the quantum theory of Lewenstein et al. [24]. These numerical calculations predict a near-bandwidth-limited isolated 530-as X-ray pulse emitted from the neon high-harmonic source within the spectral range of $90 \pm 2.5$ eV under our experimental conditions (see Fig. 7a). They also indicate the potential for even shorter pulses, if the X-ray mirror bandwidth defining the above spectral range is increased. In fact, increasing the X-ray mirror bandwidth by a factor of two in our simulations results in an 330-as X-ray pulse, accompanied by somewhat more pronounced satellites (Fig. 7b). The X-ray pulse duration cannot be significantly reduced by further increase of the mirror bandwidth under the current experimental conditions according to our simulations.

## 5    Probing atomic response and light field oscillations

The agreement of the measured X-ray pulse duration and that obtained from our numerical calculations [25] within the experimental error suggests that the timing jitter of the X-ray pulse with respect to the phase of the visible-light wave must be very small ($\ll 1$ fs) even on a sub-femtosecond time scale. As a consequence, our experiment bears evidence of the sub-femtosecond X-ray pulse being locked to the carrier wave of its generating few-cycle light pulse with attosecond precision. This indicates a surprising robustness of the high-harmonic generation process against random shifts of the absolute phase [18], i.e. of the position of the carrier with respect to the amplitude envelope. The attosecond timing stability of our sub-femtosecond X-ray pulse to a few-cycle visible-light wave makes these pulses a unique tool for investigating

the dynamic behavior of matter on an attosecond time scale. Our light-field-controlled photoemission experiment already demonstrates this capability. In the measured $\Delta W(t_{\rm d})$ it is implicit that, in the investigated spectral range near 90 eV, bound–free electronic transitions from the $4p$ state in krypton respond to X-ray excitation within less than 500 as. This is what we believe the first truly attosecond measurement.

With its duration extracted from the central part of $\Delta W(t_{\rm d})$ in Fig. 5, the X-ray pulse may now also be used to probe the evolution of the electric field in the few-cycle light pulse. The sweep of instantaneous frequency $\nu_{\rm inst}$ (or wavelength $\lambda_{\rm inst}$) in the visible-light pulse can be evaluated from the modulation in $\Delta W(t_{\rm d})$ by fitting a sinusoidal oscillation of adjustable period to the data represented by the dots in Fig. 5 over a time interval of 2.5 fs, with the sampling interval scanned through the range of $-8\,{\rm fs} \leq t_{\rm d} \leq 8\,{\rm fs}$. The dots in Fig. 5 show the carrier-frequency sweep evaluated in this manner, revealing a dynamic blue shift from a carrier wavelength of $\sim 750$ nm to $\sim 550$ nm. To understand this finding we have to remember that the light pulse used here is derived from the one generating the high harmonics.

The line in Fig. 5 is obtained from propagating a bandwidth-limited 7-fs laser pulse through the volume of neon gas emitting the high harmonics in a numerical experiment [23], and exhibits a dynamic frequency shift at the pulse center originating from self-phase modulation due to ionization of the neon gas in the harmonic source. The measured $\sim 30\%$ dynamic frequency blue shift at the center of the pulse is larger than predicted by our numerical study but reflects qualitatively the predicted behavior.

This qualitative agreement suggests that the observed blue shift can be attributed to ionization-induced self-phase modulation in the high harmonic generation process. The presence of this substantial frequency sweep in the light pulse employed for controlling X-ray photoemission provides a further strong argument for the isolated nature of our X-ray pulse: any satellite pulse of notable energy would significantly suppress fringe visibility near $t_{\rm d} = 0$, where the modulation period of the cross-correlation trace $\Delta W(t_{\rm d})$ is substantially shorter than the predicted temporal spacing of possible satellites. The achieved direct probing of the field oscillations in a light wave as implemented here is another demonstration of attosecond metrology. It will permit complete measurement of the electric field of absolute-phase-stabilized few-cycle light [24, 26].

## 6    Conclusion

With the availability of sub-femtosecond X-ray pulses, it is now possible to extend time-resolved spectroscopy into the attosecond domain by using these pulses for both triggering and probing bound–bound or bound–free transitions in atoms or molecules. However, the sub-femtosecond X-ray pulses currently available do not have sufficient fluence for X-ray-pump/X-ray-probe spectroscopy yet. Generalization of the present concept of light-field-controlled X-ray photoemission will allow us to substitute either the X-ray pump or the X-ray probe pulse by a strong few-cycle laser field without

compromising attosecond resolution. This approach vastly relaxes requirements on the X-ray pulse fluence, opening the door to attosecond spectroscopy of bound-electron dynamics with the apparatus described in this paper.

## REFERENCES

1  G. Steinmeyer, D.H. Sutter, L. Gallmann, N. Matuschek, U. Keller: Science **286**, 1507 (1999)
2  A. Baltuška, Z. Wei, M.S. Pshenichnikov, D.A. Wiersma, R. Szipöcs: Appl. Phys. B **65**, 175 (1997)
3  M. Nisoli, S. Stagira, S. De, O. Svelto, S. Sartania, Z. Cheng, M. Lenzner, Ch. Spielmann, F. Krausz: Appl. Phys. B **65**, 189 (1997)
4  U. Morgner, F.X. Kärtner, S.H. Cho, Y. Chen, H.A. Haus, J.G. Fujimoto, E.P. Ippen, V. Scheuer, G. Angelow, T. Tschudi: Opt. Lett. **24**, 411 (1999)
5  D.H. Sutter, G. Steinmeyer, L. Gallmann, N. Matuschek, F. Morier-Genoud, U. Keller, V. Scheuer, G. Angelow, T. Tschudi: Opt. Lett. **24**, 631 (1999)
6  A. Shirakawa, I. Sakane, M. Takasaka, T. Kobayashi: Appl. Phys. Lett. **74**, 2268 (1999)
7  A. L'Huillier, P. Balcou: Phys. Rev. Lett. **70**, 774 (1993)
8  C.J. Joachain, M. Dörr, N.J. Kylstra: Adv. At. Mol. Opt. Phys. **42**, 225 (2000)
9  P. Salières, A. L´Huillier, M. Lewenstein: Adv. At. Mol. Opt. Phys. **41**, 83 (1999)
10  J.J. Macklin, J.D. Kmetec, C.L. Gordon, III: Phys. Rev. Lett. **70**, 766 (1993)
11  N.A. Papadogiannis et al.: Phys. Rev. Lett. **83**, 4289 (1999)
12  P.M. Paul, E.S. Toma, P. Breger, G. Mullot, F. Augé, Ph. Balcou, H.G. Muller, P. Agostini: Science **292**, 1689 (2001)
13  M. Ivanov, P.B. Corkum, T. Zuo, A. Bandrauk: Phys. Rev. Lett. **74**, 2933 (1995)
14  I.P. Christov, M.M. Murnane, H.C. Kapteyn: Phys. Rev. Lett. **78**, 1251 (1997)
15  Ch. Spielmann, N.H. Burnett, S. Sartania, R. Koppitsch, M. Schnürer, C. Kan, M. Lenzner, P. Wobrauschek, F. Krausz: Science **278**, 661 (1997)
16  M. Drescher, M. Hentschel, R. Kienberger, G. Tempea, Ch. Spielmann, G.A. Reider, P.B. Corkum, F. Krausz: Science **291** , 1923 (2001) [published online February 15, 2001; 10 1126/science.1058561]
17  M. Hentschel, R. Kienberger, Ch. Spielmann, G.A. Reider, N. Milosevic, T. Brabec, P.B. Corkum, U. Heinzmann, M. Drescher, F. Krausz: Nature **414**, 509 (2001)
18  T. Brabec, F. Krausz: Rev. Mod. Phys. **72**, 545 (2000)
19  S. Sartania, Z. Cheng, M. Lenzner, G. Tempea, Ch. Spielmann, F. Krausz, K. Ferenc: Opt. Lett. **22**, 1562 (1997)
20  M. Schnürer, Z. Cheng, M. Hentschel, G. Tempea, P. Kálmán, T. Brabec, F. Krausz: Phys. Rev. Lett. **83**, 722 (1999)
21  M. Hentschel, Z. Cheng, F. Krausz, Ch. Spielmann: Appl. Phys. B **70**, 161 (2000)
22  U. Becker, D.A. Shirley: *VUV and Soft X-Ray Photoionization* (Plenum, New York 1996) p. 152
23  N. Milosevic, A. Scrinzi, T. Brabec: Phys. Rev. Lett. **88**, 093 905 (1996)
24  M. Lewenstein, Ph. Balcou, M.Yu. Ivanov, A. L'Huillier, P.B. Corkum: Phys. Rev. A **49**, 2117 (1994)
25  J. Itatani, F. Quéré, G.L. Yudin, M.Yu. Ivanov, F. Krausz, P.B. Corkum: Phys. Rev. Lett. **88**, 173 909 (2002)
26  A. Poppe, R. Holzwarth, A. Apolonski, G. Tempea, Ch. Spielmann, T.W. Hänsch, F. Krausz: Appl. Phys. B **72**, 373 (2001) [published online December 13, 2000; 10 1007/s003400000526]